

The effect of copper(II) salt precursor on physicochemical properties of HKUST-1 MOFs and their application as adsorbents of Cr(III) ions from aqueous solutions

Jakub Mokrzycki^{a,*}, Eliza Wolak^a, Agnieszka Orzechowska-Zieba^a, Kun Zheng^a, Dorota Duraczyńska^b, Mateusz Marzec^c, Monika Fedyna^d

^a AGH University of Krakow, Faculty of Energy and Fuels, Mickiewicza 30 Av., 30-059 Krakow, Poland

^b Jerzy Haber Institute of Catalysis and Surface Chemistry, Polish Academy of Sciences, Niezapominajek 8, 30-239 Krakow, Poland

^c AGH University of Krakow, Academic Centre for Materials and Nanotechnology, Mickiewicza 30 Av., 30-059 Krakow, Poland

^d Jagiellonian University, Faculty of Chemistry, Gronostajowa 2, 30-387 Krakow, Poland

ARTICLE INFO

Keywords:

HKUST-1
Metal-organic framework
Cr(III) adsorption
Water remediation

ABSTRACT

In this work HKUST-1 was synthesized using 4 different copper(II) salts precursors to investigate their effect on the physicochemical properties of obtained metal-organic frameworks (MOFs). To allow greener synthesis of HKUST-1, *N,N*-dimethylformamide-free (DMF-free) procedure was employed. Copper nitrate, copper sulphate, copper acetate, and copper chloride were selected for the syntheses. The yield of obtained products changed in order acetate>nitrate>sulfate, whereas synthesis with copper chloride yielded no product after 24 h at 110 °C hydrothermal treatment. The obtained materials were characterized by means of XRD, N₂ adsorption–desorption at 77 K, TG, SEM, FTIR, DLS, and XPS. MOFs were further investigated as adsorbents of Cr(III) ions from aqueous solutions. Adsorption kinetics and adsorption statics models were correlated with the experimental data to gain a better understanding of the adsorption effectiveness.

1. Introduction

Metal-organic frameworks (MOFs) are a new group of materials that appeared in the late 1990s. MOFs are porous, crystalline solids composed of cations or metal clusters (acting as metal centers or nodes) and organic ligands (acting as bridges between these nodes), connected to each other by coordination bonds. The coordination bonds between the metal and the ligand are strong, resulting in an open, crystalline structures that remain stable when the molecules inside are removed, thus creating a porous material. Those compounds with an organic-inorganic structure are also referred as porous network coordination polymers (PCP) (porous coordination polymers). Due to their highly ordered structure, porosity, elevated internal surface areas, chemical stability and designable structures, MOFs have gained attention in the last twenty years [1]. Owing to their unique properties, MOFs have found numerous applications in various fields including gas adsorption/sequestration [2], adsorption of organic pollutants [3], catalysis [4], sensors [5], and drug delivery [6].

HKUST-1 (Hong Kong University of Science and Technology-1), also

known as MOF-199 or Cu₃(BTC)₂, is a crystalline structure obtained from coordination of Cu²⁺ clusters with organic linker 1,3,5-benzenetricarboxylic acid (H₃BTC). HKUST-1 forms a regular, three-dimensional material, characterized by a large specific surface area > 1000 m² g⁻¹ and pore window of about 0.9 nm [7]. In a typical synthesis route, copper(II) salt precursor (nitrate [8], or acetate [9]) is dissolved in water, while H₃BTC is dissolved in DMF (*N,N*-dimethylformamide) [10], alcohol (methanol [11], ethanol [12]), or their mixtures [13]. The solutions are then mixed together under various regimes. The process conditions *i.e.* temperature, reaction time, selected synthesis method, and addition of modulators, affects the yield, and physicochemical properties of the final product [14,15]. Liu et al. [16] investigated the effect of different salt precursors and addition of triethylamine (TEA) on the properties of obtained HKUST-1 materials. Both salt precursor and addition of modulator significantly affected the yield of MOFs and their properties: specific surface area, pore volume, and benzene oxidation yield. In fact, modulators allow to obtain highly regular products with uniform crystal sizes, however the need of their removal from the material in post-synthesis procedure increase the cost of MOFs production.

* Corresponding author.

E-mail address: jmokrzycki@agh.edu.pl (J. Mokrzycki).

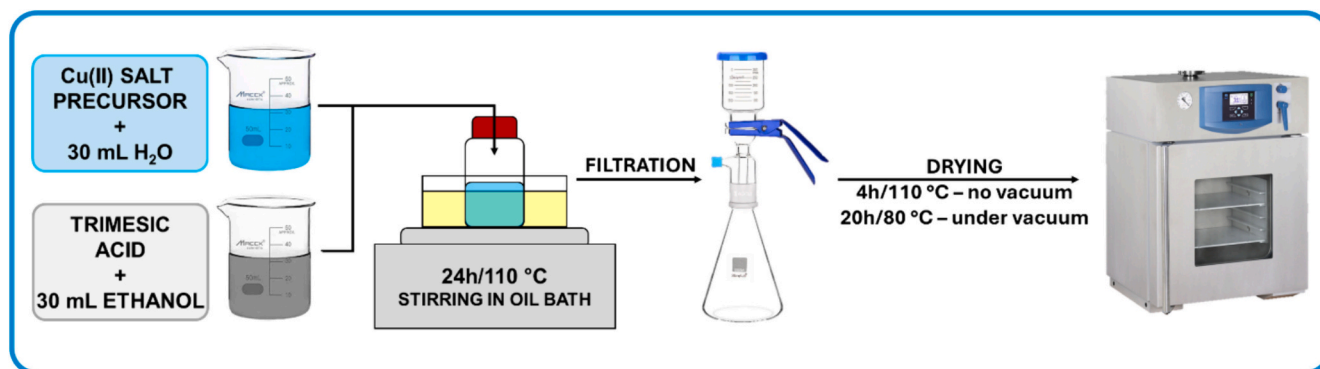


Fig. 1. HKUST-1 synthesis scheme.

An important factor, which guides the crystal growth is the speed of organic linker deprotonation, which was evidenced to be fast, when as a copper(II) precursor $\text{Cu}(\text{OH})_2$ was used, with simultaneous elimination of necessity of NO_3^- or Cl^- ions removal from the reaction medium [17]. The most common method of MOFs synthesis is a solvothermal method, in which the process is carried out in a closed vessel, with a well dispersion of reactants allowing to obtain a sufficient yield and quantity of the product. This method can be modified by assistance of ultrasounds (sonochemical method) [18], or microwaves [19,20], which affects the nucleation and further crystal growth, and was also reported to improve the specific surface area. A solvent-free synthesis *i.e.* mechanochemical method *via* grinding the reactants was also reported [21].

Due to unique and regular structure, HKUST-1 has found numerous applications in gas separation and storage [22], catalysis [23], and water remediation [24]. In case of catalysis, the application of MOFs is rather limited, due to relatively low thermal stability $<300^\circ\text{C}$. However, their adsorption properties have been intensively studied in recent years [25]. On the other hand, in terms of application of HKUST-1 in aqueous solutions, owing to high hydrophilicity of the material, it was reported that its structure can be irreversibly changed while being exposed to even mild temperatures of about 50°C [26]. Xing et al. [27], have also investigated the HKUST-1 materials as adsorbents of pharmaceuticals and their stability in water. HKUST-1 structure was completely destroyed after 2 week water exposure, while composite materials HKUST-1/ZnO were characterized by enhanced stability.

Chromium is classified as one of the most abundant heavy metals on Earth [28]. Its most common valence forms are +3 and +6, which vary in terms of their toxicity. Both trivalent (Cr(III)) and hexavalent chromium (Cr(VI)) are biocompatible, so they can be easily transferred to the living organisms and can accumulate in cells. While Cr(III) has a positive effect on the living organisms (to a certain extend) as it participates in regulation of glucose metabolism, lipids and proteins homeostasis, Cr(VI) is considered as toxic form of chromium, which can cause kidney, lungs or liver cancers [29]. Also, according to World Health Organisation (WHO) the acceptable levels of total chromium in drinking water should not exceed 0.05 mg L^{-1} [30]. Cr(III) is from 100 to 300-fold less toxic than Cr(VI), however it should be noted that greater amounts of Cr(III) can even lead to anaemia due to competition with iron ions, or affect calcium metabolism in bones. There is also a danger of valence form change within the living organism from Cr(III) to Cr(VI), which can bring a negative health effect [31]. For such reasons, the need of chromium elimination from the environment (mostly water) has become an emerging topic for scientists. Among methods of chromium removal: electrodialysis [32], membrane technologies [33], or coagulation [34], adsorption is considered as the cheapest and most efficient [35].

In present study, HKUST-1 was synthesized using 4 different copper (II) salts precursors *i.e.* nitrate, sulfate, acetate, and chloride. To allow a greener synthesis, the procedure of organic linker dissolution was free from DMF, and only ethanol was used as organic solvent. Furthermore,

no additional modulators were used. The obtained HKUST-1 materials were characterized in detail by means of XDR, FTIR, SEM, TG, N_2 adsorption-desorption, particle size analysis, and XPS to gain a better understanding of the salt precursor effect on the product yield, and physicochemical properties. As a potential utility, the series of obtained materials were evaluated as adsorbents of Cr(III) ions from aqueous solutions. The results of experimental data were correlated with the adsorption kinetics and adsorption statics models to evaluate their effectiveness in the investigated process. To the best of the authors knowledge, such comparison was not demonstrated in the literature until now and there are limited works about removal of Cr(III) ions using MOFs.

2. Materials and methods

2.1. HKUST-1 syntheses

The syntheses of the HKUST-1 were conducted following the modified procedure described by Chen et al. [8]. Briefly, 5 mmol of trimesic acid (Sigma Aldrich, Burlington, MA, USA) was dissolved in 30 mL of ethanol (96 % purity, Stanlab, Lublin, Poland). In a separate beaker, appropriate amount of copper(II) salt: $(\text{CH}_3\text{COOH})_2\text{Cu}\cdot\text{H}_2\text{O}$ (Fluka, Buchs, Switzerland), $\text{CuCl}_2\cdot 2\text{H}_2\text{O}$ (Sigma Aldrich, Burlington, MA, USA), $\text{Cu}(\text{NO}_3)_2\cdot 3\text{H}_2\text{O}$ (Aktyn, Suchy Las, Poland), or $\text{CuSO}_4\cdot 5\text{H}_2\text{O}$ (Sigma Aldrich, Burlington, MA, USA), was weighed in an amount that equaled to 9 mmol of Cu(II) ions. Copper(II) salt was dissolved in 30 mL of demineralized water. Next, 2 solutions were mixed together in a glass hydrothermal reactor, equipped with magnetic stirrer and placed in an oil bath. Solution was vigorously stirred for 24 h at $110 \pm 1^\circ\text{C}$. The solid product was filtrated and washed several times with distilled water to remove impurities and dried in a vacuum oven. MOFs were denoted as HKUST-1-Ac, HKUST-1-C, HKUST-1-N, and HKUST-1-S, where the letters correspond to the used copper(II) salt precursors: acetate (Ac), chloride (C), nitrate (N), and sulfate (S), respectively. The procedure of samples preparation is demonstrated in Fig. 1.

2.2. Characterization methods

2.2.1. X-ray diffraction (XRD)

X-ray diffraction (XRD) measurements were conducted to determine phase composition of MOFs. PANalytical Empyrean diffractometer was employed (Malvern Panalytical, Malvern, UK) and the radiation source was $\text{CuK}\alpha$ $\lambda = 1.5406\text{ \AA}$. The 2θ range varied from 5° to 45° , with a 0.013° step.

2.2.2. N_2 adsorption-desorption at -196°C

Adsorption-desorption of nitrogen at -196°C was performed using the ASAP 2020 instrument (Micromeritics, Norcross, GA, USA). The specific surface area (S_{BET}), total pore volume (V_t), and micropore

Table 1
Adsorption kinetics and adsorption statics models.

| Adsorption kinetics | | |
|---------------------|--|---|
| Model | Equation | Symbol explanation |
| Pseudo-first order | $\ln(q_{exp} - q_t) = \ln(q_{eq}) - k_1 t$ | t – time, min q_{exp} – amount adsorbed as obtained from t/q_t graph, mg g^{-1} q_t – amount adsorbed at time t , mg g^{-1} q_{eq} – amount adsorbed derived from equation, mg g^{-1} k_1 – model constant of adsorption, min^{-1} |
| Pseudo-second order | $\frac{t}{q_t} = \frac{1}{k_2 * q_{eq}^2} + \frac{t}{q_{eq}}$ | t – time, min q_t – amount adsorbed at time t , mg g^{-1} q_{eq} – amount adsorbed at equilibrium mg g^{-1} k_2 – model constant of adsorption, $\text{g mg}^{-1} \text{min}^{-1}$ |
| Bangham | $\log\left[\log\left(\frac{C_0}{C_0 - q_t * m}\right)\right] = \log\left(\frac{k_0 * m}{2.303 * V}\right) + \log(t)$ | t – time, min q_t – amount adsorbed at time t , mg g^{-1} C_0 – initial concentration in solution, mg L^{-1} k_0 – Bangham model constant, $\text{L}^2 \text{g}^{-1}$ α – Bangham model constant, – V – solution volume, L m – mass of adsorbent per solution litre, g L^{-1} |
| Elovich | $q_t = \frac{1}{b} \ln(a * b) + \frac{1}{b} \ln(t)$ | t – time, min q_t – amount adsorbed at time t , mg g^{-1} a – initial adsorption rate constant, $\text{mg g}^{-1} \text{min}^{-1}$ b – Elovich model constant, g mg^{-1} |
| Adsorption statics | | |
| Model | Equation | Symbol explanation |
| Langmuir | $\frac{C_{eq}}{q_{eq}} = \frac{C_{eq}}{q_{max}} + \frac{1}{K_L * q_{max}}$ | q_{eq} – amount adsorbed by adsorbent at equilibrium, mg g^{-1} C_{eq} – the equilibrium concentration in solution, mg L^{-1} q_{max} – monolayer capacity of the adsorbent, mg g^{-1} K_L – the Langmuir adsorption constant, L mg^{-1} |
| Freundlich | $\ln(q_{eq}) = \ln(K_F) + \frac{1}{n} \ln(C_{eq})$ | q_{eq} – amount adsorbed by carbon at equilibrium, mg g^{-1} C_{eq} – the equilibrium concentration in solution, mg L^{-1} K_F – the Freundlich constant, $\text{mg}^{1-1/n} \text{L}^{1/n} \text{g}^{-1}$ $1/n$ – heterogeneity factor, - |

Table 2
Reaction pH and yield of HKUST-1 syntheses.

| Parameters | HKUST-1-Ac | HKUST-1-C | HKUST-1-N | HKUST-1-S |
|--------------------|-------------|-------------|-------------|-------------|
| pH of synthesis | 3.92 ± 0.03 | 2.30 ± 0.03 | 2.96 ± 0.05 | 1.79 ± 0.04 |
| Synthesis yield, % | 100.8 | 0 | 97.4 | 23.1 |

volume (V_{micro}) were calculated from adsorption-desorption isotherms using MicroActive V 4.06 software (Micromeritics Norcross, GA, USA). The V_t was estimated from the adsorbed volume at p/p_0 of approx. 0.90. The H–K method was used to determine the V_{micro} values. Prior to the analysis, samples were degassed at 150 °C for 12 h to remove remaining within the pores of HKUST-1 materials solvents.

2.2.3. Fourier-transform infrared spectroscopy (FTIR)

The Fourier-transform infrared spectra of investigated samples were collected using a spectrometer (Nicolet 6700, ThermoScientific, Madison, WI, USA) in Attenuated Total Reflection mode (ATR-FTIR), operating in a wavenumbers from 3900 to 650 cm^{-1} .

2.2.4. Thermogravimetric analysis (TGA)

Thermogravimetric analysis (TG) was performed by means of Q5000IR apparatus (TA Instruments, New Castle, DE, USA). HKUST-1 sample was weighed (about 30 mg) and heated from RT to 700 °C in argon flow of 100 mL min^{-1} with a heating rate of 5 °C min^{-1} .

2.2.5. Scanning electron microscopy (SEM)

SEM was employed to gain a better understanding of the surface morphology of obtained MOFs. Prior to the imaging, samples were coated with a 30 nm layer of chromium using K575X Turbo Sputter

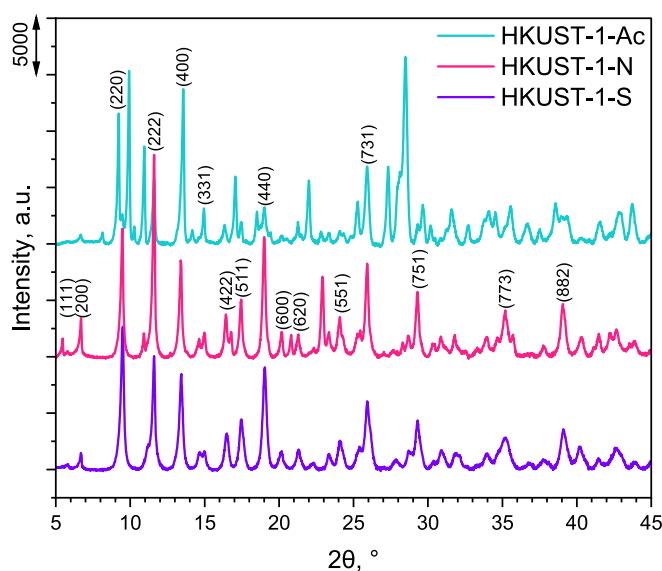


Fig. 2. XRD patterns of investigated MOFs.

Coater (Quorum Emitech, South Stour Avenue, Ashford, UK). Images were collected using JEOL JSM 7500 F (JEOL, Tokyo, Japan). Additional TEM imaging was conducted for HKUST-1-S sample. The methodology is provided in the Supplementary Information.

2.2.6. Particle size analysis via dynamic light scattering (DLS)

The analysis of particle size of obtained materials was conducted using a laser-diffraction analyzer Mastersizer 3000 (Malvern

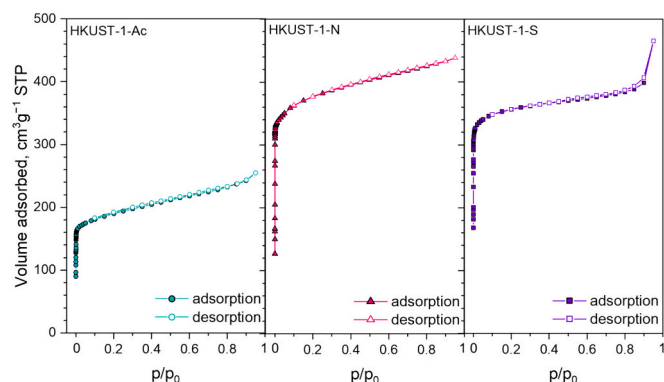


Fig. 3. N_2 adsorption-desorption isotherms at $-196\text{ }^\circ\text{C}$ of investigated MOFs.

Table 3

Surface properties of investigated MOFs.

| Parameters | HKUST-1-Ac | HKUST-1-N | HKUST-1-S |
|---------------------------------|------------|-----------|-----------|
| $S_{\text{BET}}, m^2 g^{-1}$ | 961 | 1453 | 1790 |
| $V_t, cm^3 g^{-1}$ | 0.418 | 0.671 | 0.688 |
| $V_{\text{micro}}, cm^3 g^{-1}$ | 0.398 | 0.622 | 0.636 |

Panalytical, Malvern, UK).

2.2.7. X-ray photoelectron spectroscopy analysis (XPS)

The XPS analyses were carried out in a PHI VersaProbeII Scanning XPS system using monochromatic $Al K\alpha$ (1486.6 eV) X-rays focused to a $100\text{ }\mu\text{m}$ spot and scanned over the area of $400\text{ }\mu\text{m} \times 400\text{ }\mu\text{m}$. The photoelectron take-off angle was 45° and the pass energy in the analyzer was set to 117.50 eV for survey scans and 46.95 eV to obtain high energy resolution spectra for the C 1s, O 1s, Cu 2p and Cr 2p regions. A dual beam charge compensation with 7 eV Ar^+ ions and 1 eV electrons were used to maintain a constant sample surface potential regardless of the sample conductivity. All XPS spectra were charge referenced to the unfunctionalized, saturated carbon (C—C) C 1s peak at 285.0 eV. The operating pressure in the analytical chamber was $<3 \cdot 10^{-9}$ mbar. Deconvolution of spectra was carried out using PHI MultiPak software (v.9.9.3). Spectrum background was subtracted using the Shirley method.

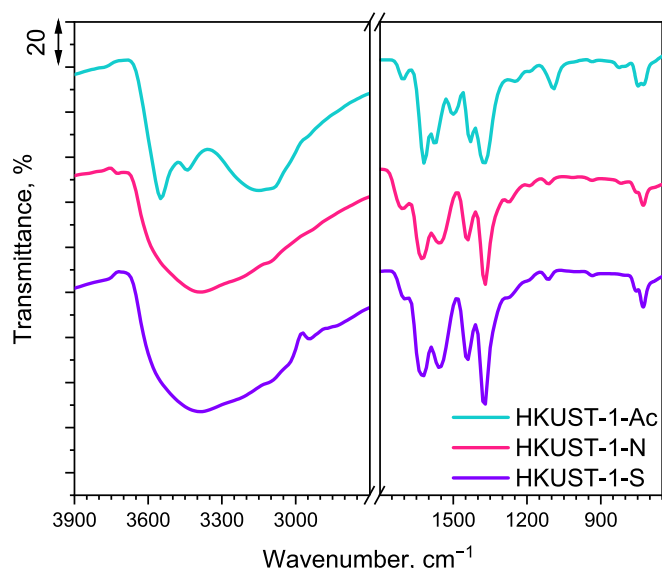


Fig. 4. FTIR analysis of investigated MOFs.

2.3. Cr(III) ions adsorption

Adsorption of Cr(III) ions was conducted according to the following procedure. Prior to the adsorption, materials were dried for 1 h in oven at $110\text{ }^\circ\text{C}$.

Adsorption kinetics studies were conducted to investigate the effect of adsorption time needed to obtain saturation. As Cr(III) ions precursor, $Cr(NO_3)_3 \cdot 9H_2O$ (Honeywell-Fluka, Bucharest, Romania) was used. The Cr(III) ions solution initial concentration was $300\text{ mg Cr(III) L}^{-1}$ and the pH was adjusted to 5.00. Briefly, 200 mg of HKUST-1 sample was weighed in an Erlenmeyer flask and mixed with 200 mL of solution using a magnetic stirrer. Samples were collected from the same flask through the time of the experiment at defined time intervals (5, 10, 15, 30, 45, 60, 90, 120, 150, and 180 min) and filtrated. Each experiment was conducted in duplicate.

Adsorption statics studies were conducted to investigate the effect of Cr(III) ions initial concentration on the adsorption capacity at equilibrium. The selected initial concentrations were: 30, 60, 90, 120, 150, 200, 300, and $400\text{ mg Cr(III) L}^{-1}$. All the solutions pH were adjusted to 5.00. Briefly, 100 mg of HKUST-1 sample was weighed in an Erlenmeyer flask and mixed with 200 mL of solution of defined initial concentration, using a magnetic stirrer. Samples were collected after 120 min of mixing and filtrated. Each experiment was conducted in duplicate.

The concentration of Cr(III) ions was determined using UV-Vis spectrophotometer UV-5600 (Shanghai Matash Instruments, Shanghai, China) at wavelength of 540 nm. Prior to the measurement, 4 mL of filtrated sample was collected and mixed with 0.095 g of disodium

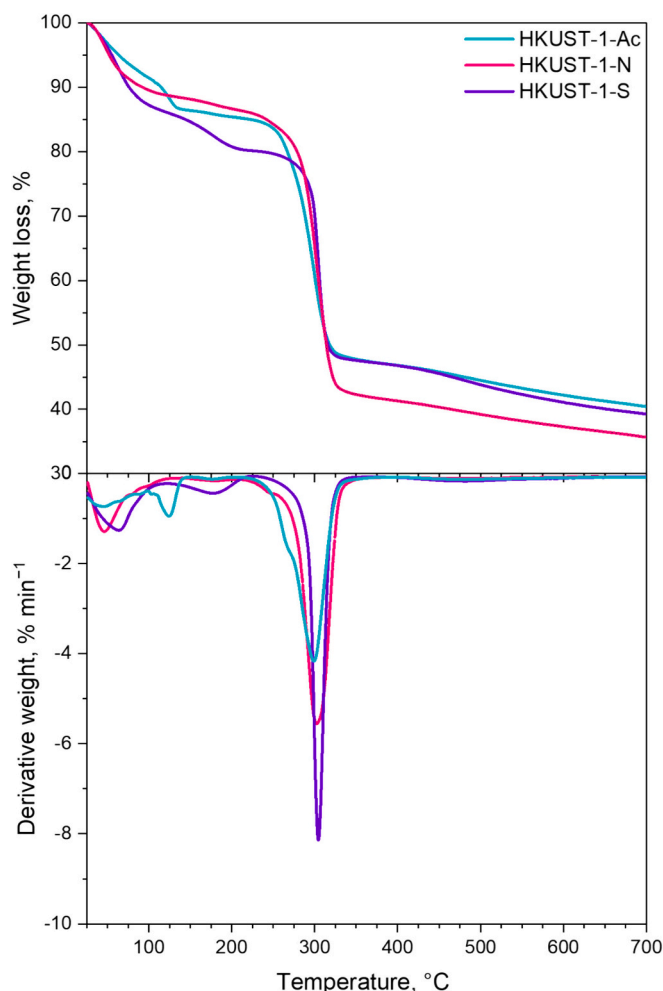


Fig. 5. TG and DTG curves of investigated MOFs.

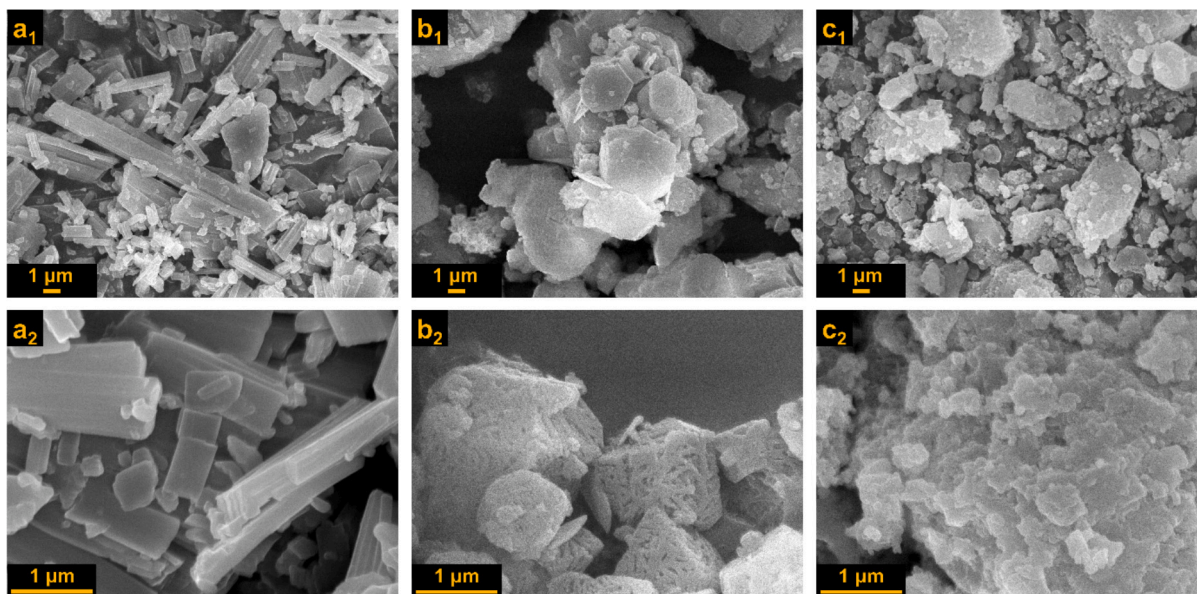


Fig. 6. SEM images of investigated MOFs: HKUST-1-Ac (a), HKUST-1-N (b), and HKUST-1-S (c), with magnification of 5000 (1), and 25,000 (2).

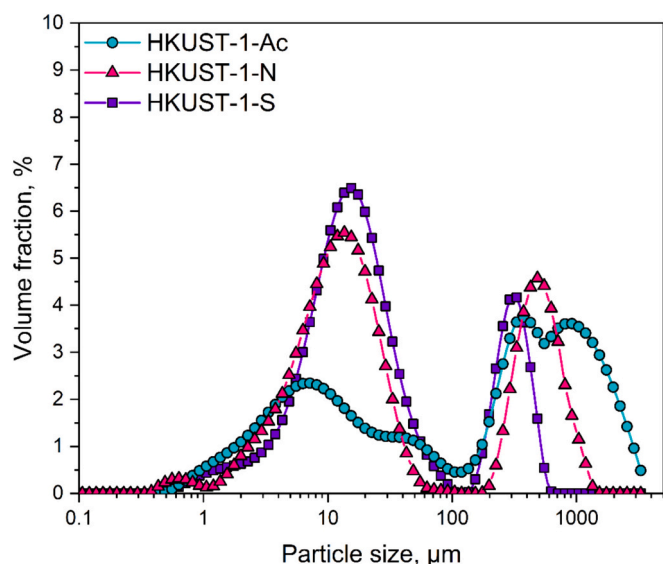


Fig. 7. DLS particle size analysis of investigated MOFs.

versenate dihydrate (Avantor, Gliwice, Poland) and placed into a water bath at $75 \pm 2^\circ\text{C}$ for 10 min to obtain a purple complex of Cr(III) ions with EDTA. The adsorption capacity at equilibrium (q_{eq}) or at defined time (q_t) was calculated using Eq. (1).

$$q_{eq} \text{ or } q_t = \frac{(C_0 - (C_{eq} \text{ or } C_t)) \cdot V}{m} \cdot 100\% \quad (1)$$

where, q_{eq} , q_t – adsorption capacity at equilibrium or time (t , min), (mg g^{-1}); C_0 , C_{eq} , C_t – initial, equilibrium or at defined time (t) concentrations of Cr(III) ions, (mg L^{-1}); V – volume of solution used for adsorption, (L); m – mass of adsorbent, (g).

Adsorption kinetics was studied by using kinetic models: pseudo-first order, and pseudo-second order, while adsorption statics was studied by using Langmuir, and Freundlich models, to allow comparison of the calculated values with those obtained from the experiments [35]. The linearization of the models is summarized in Table 1.

3. Results and discussion

3.1. Materials characteristics

Many factors can affect MOFs synthesis *i.e.* temperature, time, solution pH, stirring, co-existing ions, addition of modulators, assistance of ultrasounds/microwaves. By sufficient adjustment of these parameters, it is possible to control the desired properties of the obtained MOFs. HKUST-1 solvothermal synthesis used in present study allows to obtain high surface area materials, due to well dispersion of reactants in the reaction medium [36].

The products yield is presented in Table 2. The effect of co-existing ions originating from the copper(II) salt precursor significantly affected the synthesis yield of HKUST-1. Synthesis using copper(II) chloride appeared to block the reaction as there was no product obtained after the synthesis. Synthesis using copper(II) acetate appeared to yield the highest amount of the product with nearly 100 % conversion. Slightly $>100\%$ product yield of HKUST-1-Ac, can be a result of partial incorporation of acetic ions originating from the salt precursor into the HKUST-1 crystalline structure during the crystal growth *via* ligand exchange between AcO^- and BTC^{3-} ions and/or incomplete removal of solvent [37,38]. Conventionally used for HKUST-1 synthesis copper(II) nitrate allowed to obtain 97.4 % product yield. As for copper(II) sulfate, the product yield was rather low and as high as 23.1 %. The synthesis pH had rather insignificant effect on the product yield and was related to the dissociation of salt precursor in the reaction medium.

The phase composition of obtained MOFs is presented in Fig. 2. The characteristic refraction peaks which are located at $2\theta = 5.44, 6.69, 9.47, 10.90, 11.61, 13.38, 14.97, 16.43, 17.44, 19.00, 20.17, 21.25, 22.90, 24.09, 25.92, 29.31, 35.21, \text{ and } 39.06^\circ$, corresponding to the crystal planes: (111), (200), (220), (222), (400), (331), (422), (511), (440), (600), (620), (551), (731), (751), (773), and (882), respectively clearly confirmed the structure of HKUST-1. Their positions stay in line with the PDF-4+ powder diffraction database (JCPDS 00-064-0936) [39]. Depending on the used Cu precursor, the occurrence and/or intensities of certain peaks varied among the samples. Syntheses using copper(II) nitrate (HKUST-1-N) and copper(II) sulfate (HKUST-1-S), allowed to obtain comparable HKUST-1 structures with no additional peaks. On the other hand, for HKUST-1-Ac additional peaks appeared, which might be attributed to undefined HKUST-1 planes [40]. Acetate

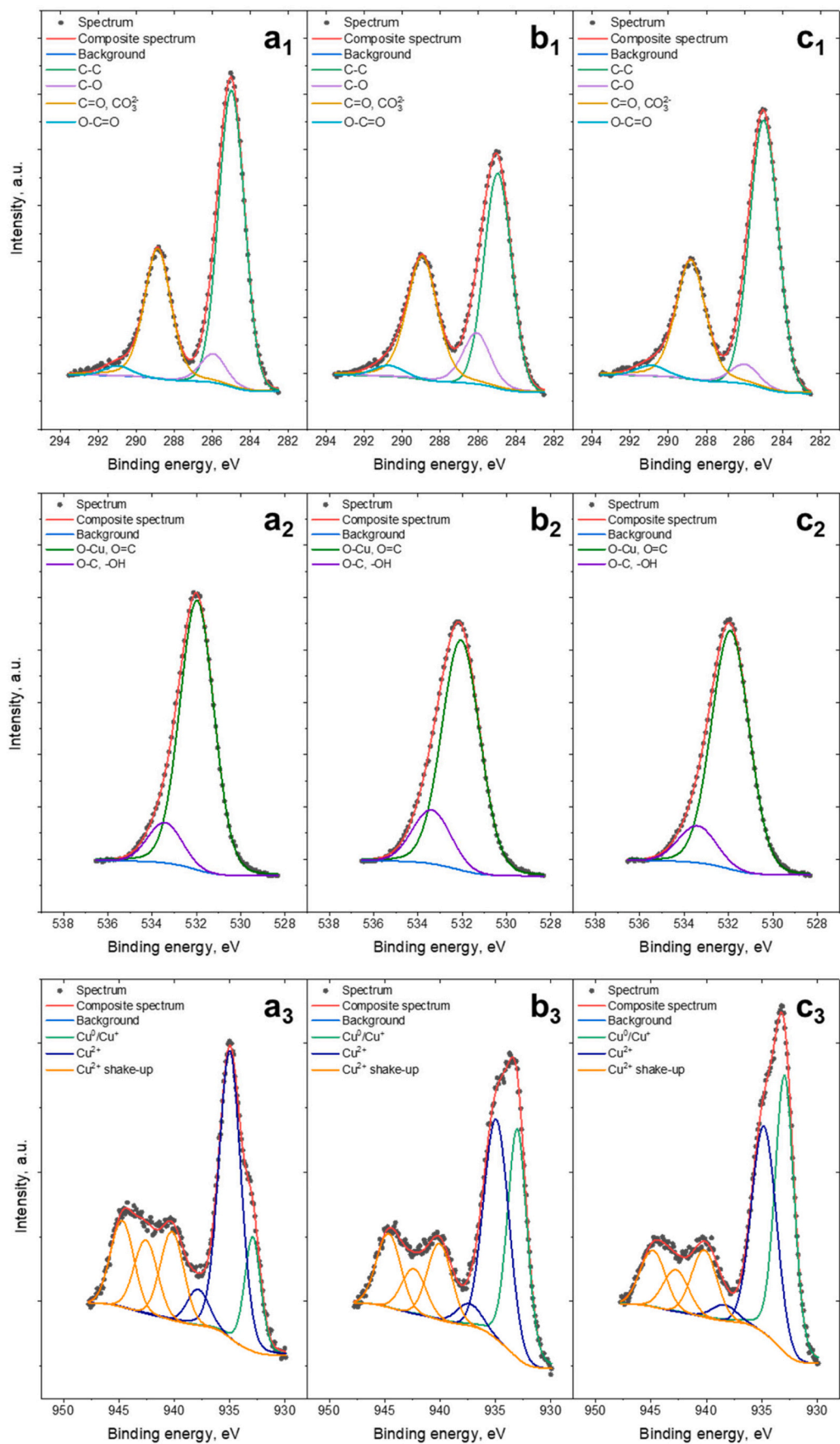


Fig. 8. XPS spectra of C 1s (a₁–c₁), O 1s (a₂–c₂), and Cu 2p (a₃–c₃) for HKUST-1-Ac (a), HKUST-1-N (b), and HKUST-1-S (c) samples.

Table 4

Adsorption kinetic models parameters of Cr(III) ions adsorption using investigated MOFs.

| Model | Kinetic parameters | HKUST-1-Ac | HKUST-1-N | HKUST-1-S |
|---------------------|-----------------------------|------------|-----------|-----------|
| Pseudo first order | $q_{exp}, mg\ g^{-1}$ | 48.077 | 67.114 | 68.027 |
| | $q_{eq}, mg\ g^{-1}$ | 28.199 | 45.101 | 39.504 |
| | k_1, min^{-1} | 0.043 | 0.015 | 0.028 |
| | R^2 | 0.959 | 0.980 | 0.938 |
| Pseudo second order | $q_{eq}, mg\ g^{-1}$ | 48.077 | 67.114 | 68.027 |
| | $k_2, g\ mg^{-1}\ min^{-1}$ | 0.004 | 0.001 | 0.002 |
| | R^2 | 0.999 | 0.993 | 0.998 |
| Bangham | α | 0.185 | 0.319 | 0.189 |
| | $k_0, L^2\ g^{-1}$ | 0.014 | 0.009 | 0.020 |
| | R^2 | 0.865 | 0.973 | 0.966 |
| Elovich | $a, mg\ g^{-1}\ min^{-1}$ | 98.877 | 12.838 | 91.224 |
| | $b, g\ mg^{-1}$ | 0.161 | 0.085 | 0.109 |
| | R^2 | 0.900 | 0.980 | 0.934 |

ions present in the reaction medium, act as capping agent during MOF self-assembly process, and can be incorporated into the MOF structure by coordination bonding with metal clusters or terminated ligands [41]. Such behavior can significantly change the crystalline planes of obtained MOF, which was evidenced in HKUST-1-Ac XRD pattern. The material did not become amorphous despite the high share of acetate ions in the synthesis solution [42]. Peaks, that occurred for HKUST-1-Ac sample, were not assigned as HKUST-1 phase, which can be a result of formation of additional phase of $Cu_2OH(BTC)(H_2O)_n \cdot 2nH_2O$ also reported by Crawford et al. [43]. Additional peaks at $2\theta = 8.14, 9.22, 9.92, 14.17, 17.05, 18.51, 22.81, 28.48, 32.74^\circ$ stay in line with the reports of Loera-Serna et al. [44].

In Fig. 3 the isotherms of nitrogen adsorption-desorption at $-196^\circ C$ are compared. The adsorption isotherm shape was identified as type IA according to IUPAC classification, typical for microporous materials. Small hysteresis loop type H4, often obtained for micro-mesoporous materials was observed for sample HKUST-1-S [45]. The surface properties information is summarized in Table 3. All the materials were microporous as was evidenced by the volume of micropores (V_{micro}) calculated using H-K method, which account from 92.4 to 95.2% of all pores types. HKUST-1-S was characterized by the highest specific surface area (S_{BET}) of $1790\ m^2\ g^{-1}$, whereas HKUST-1-Ac the lowest ($961\ m^2\ g^{-1}$). Crystal imperfections were reported to lower the specific surface area of the HKUST-1 MOFs [46]. The total pore volume changed in order: $0.418 < 0.671 < 0.688\ cm^3\ g^{-1}$ for HKUST-1-Ac < HKUST-1-N < HKUST-1-S, respectively and is consistent with the already reported materials [47]. Furthermore, the procedure involving vacuum drying of the MOFs appears to not cause damage to the structure.

The FTIR spectra of investigated samples are presented in Fig. 4. In the region of wavenumber from 1800 to $650\ cm^{-1}$, it can be seen, that all

MOFs, displayed familiar shape of spectra with characteristic for HKUST-1 bands. Band assigned to stretching vibrations of Cu – O is located at $726\ cm^{-1}$, asymmetric stretching vibrations of –COO can be seen at 1630 and $1440\ cm^{-1}$ and symmetric stretching vibrations of –COO at $1370\ cm^{-1}$ [48]. The band at $1090\ cm^{-1}$ occurred from C – O – Cu stretching vibrations, as was also evidenced by Khader et al. [49]. Small band at about $1710\ cm^{-1}$ also confirms the presence of 1,3,5-tricarboxylic acid [50]. In the region of wavenumber from 3900 to $2700\ cm^{-1}$, a broad peak assigned as stretching vibrations of O – H. For HKUST-1-Ac the peak of O – H can be distinguished into 3 peaks with maxima at $3550, 3440,$ and $3150\ cm^{-1}$, which implies occurrence of loosely bonded water molecules into the MOF structure [51,52].

Thermogravimetric analysis (TGA) was conducted to gain a better understanding of the thermal stability of MOFs. The results of TGA and derivative TG (DTG) are presented in Fig. 5. For all samples, from 2 to 3 stages of weight loss were obtained. First weight loss with a maximum at about $50^\circ C$ was identified as loss of solvent (ethanol and water) remaining within the pores of the material after the synthesis. Second weight loss, which was obtained at about $300^\circ C$, originated from the HKUST-1 decomposition. Its position remains in line with the literature reports [53,54]. Additional weight loss seen at about $125^\circ C$ for HKUST-1-Ac can be related to water removal from the $Cu_2OH(BTC)(H_2O)_n \cdot 2nH_2O$ phase [43]. For HKUST-1-S a small additional peak at about $155^\circ C$ was probably related to release of water adsorbed in pores, due to its highest specific surface area among the investigated series (see Table 3).

In Fig. 6 the SEM images of obtained HKUST-1 materials are summarized. It can be seen, that by changing the copper(II) salt precursor, the morphology of MOFs varied significantly. For HKUST-1-Ac (Fig. 6a₁ and 6a₂), the obtained crystals were layered rods shaped. The crystals shape appeared to be the most regular among investigated HKUST-1 series. Also, the synthesis pH for this sample was the highest among the investigated materials (3.92 – see Table 2). Acetate ions act as capping agent in the MOFs synthesis and fasten the nucleation by initialization of particle formation at early stages of the synthesis, as was also evidenced by Guo et al. [42]. The authors obtained similar MOF

Table 5

Adsorption static models parameters of Cr(III) adsorption using investigated MOFs.

| Model | Static parameters | HKUST-1-Ac | HKUST-1-N | HKUST-1-S |
|------------|------------------------------------|------------|-----------|-----------|
| Langmuir | $q_{max}, mg\ g^{-1}$ | 46.512 | 76.923 | 84.034 |
| | $K_L, L\ mg^{-1}$ | 0.040 | 0.036 | 0.044 |
| | R^2 | 0.967 | 0.989 | 0.958 |
| Freundlich | $K_F, mg^{1-1/n}\ L^{1/n}\ g^{-1}$ | 8.488 | 12.065 | 28.199 |
| | $1/n$ | 0.302 | 0.330 | 0.180 |
| | R^2 | 0.881 | 0.836 | 0.799 |

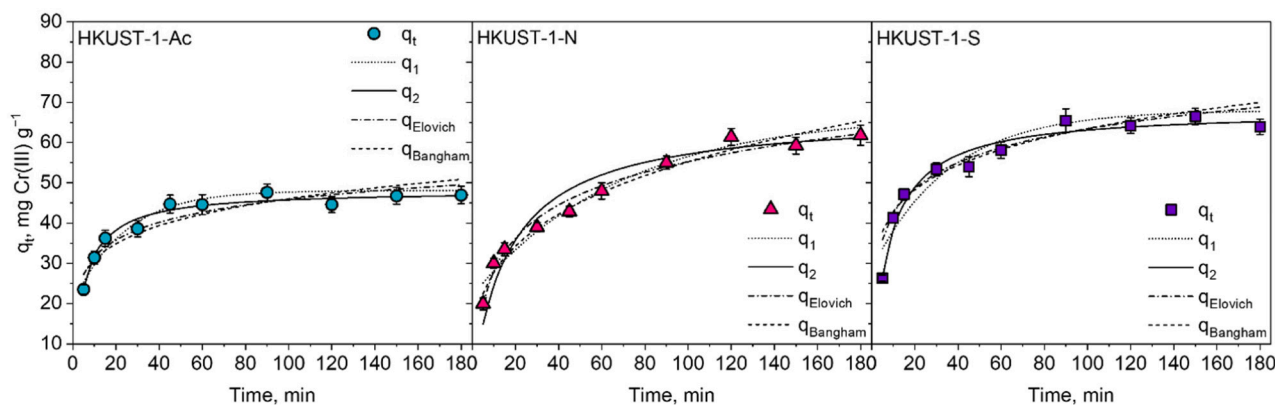


Fig. 9. Cr(III) ions adsorption kinetics correlation of experimental data with pseudo-first order (dot line – q_1), pseudo-second order (solid line – q_2), Elovich (dash-dot line – $q_{Elovich}$), and Bangham (dash line – $q_{Bangham}$) models.

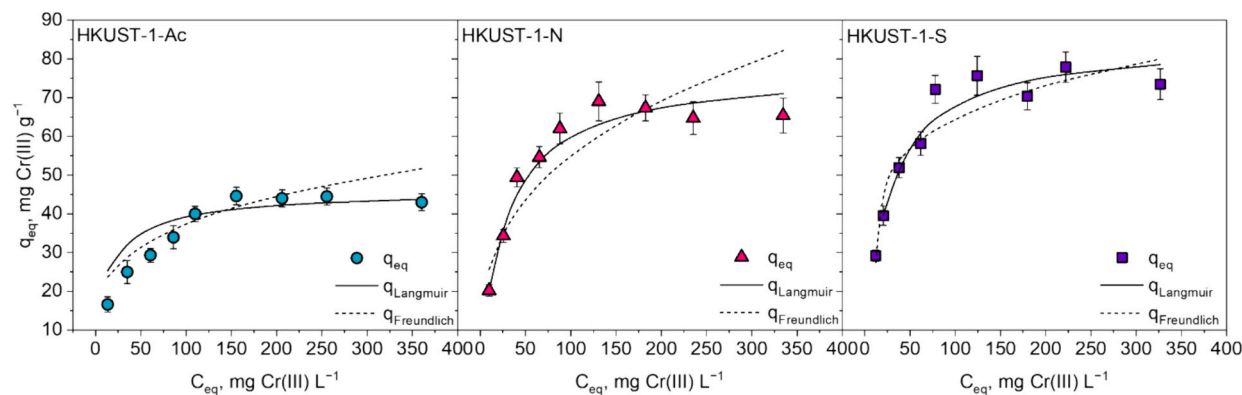


Fig. 10. Cr(III) ions adsorption statics correlation of experimental data with Langmuir (solid line - q_{Langmuir}) and Freundlich (dash line - $q_{\text{Freundlich}}$) models.

Table 6
Comparison of adsorption capacities towards Cr(III) ions removal using various materials.

| Adsorbent | Adsorption parameters | Adsorption capacity | Reference |
|--|---|------------------------------|------------|
| HKUST-1 | Initial Cr(III) ions concentration: 1000 mg L ⁻¹ Temperature: 25 °C Adsorbent dose: 1 g L ⁻¹ Adsorption pH: 6 | 65.0 mg g ⁻¹ | [66] |
| HKUST-1 | Initial Cr(III) ions concentration: 5–80 mg L ⁻¹ Temperature: 15–35 °C Adsorbent dose: 2 g L ⁻¹ Adsorption pH: 6 | 23.4–24.6 mg g ⁻¹ | [67] |
| Muscovite mica | Initial Cr(III) ions concentration: 5–50 mg L ⁻¹ Temperature: 30–90 °C Adsorbent dose: 1 g L ⁻¹ Adsorption pH: 7 | 4.9–15.6 mg g ⁻¹ | [68] |
| Hornwort (<i>Ceratophyllum demersum</i> L.) derived biochar | Initial Cr(III) ions concentration: 25–300 mg L ⁻¹ Temperature: 25 °C Adsorbent dose: 1 g L ⁻¹ Adsorption pH: 5 | 63.7 mg g ⁻¹ | [69] |
| HKUST-1-S | Initial Cr(III) ions concentration: 30–400 mg L ⁻¹ Temperature: 25 °C Adsorbent dose: 1 g L ⁻¹ Adsorption pH: 5 | 84.0 mg g ⁻¹ | This study |
| HKUST-1-N | Initial Cr(III) ions concentration: 30–400 mg L ⁻¹ Temperature: 25 °C Adsorbent dose: 1 g L ⁻¹ Adsorption pH: 5 | 76.9 mg g ⁻¹ | |
| HKUST-1-Ac | Initial Cr(III) ions concentration: 30–400 mg L ⁻¹ Temperature: 25 °C Adsorbent dose: 1 g L ⁻¹ Adsorption pH: 5 | 46.5 mg g ⁻¹ | |

morphology by adding sodium acetate to the synthesis. As for the syntheses using copper(II) nitrate (Fig. 6b₁ and b₂) and copper(II) sulfate (Fig. 6c₁ and c₂), the morphology appeared to be highly irregular. The crystals aggregated into bigger clusters and it is difficult to define their shape. Such phenomenon might be related to the synthesis conditions, in which the solution was vigorously stirred through the entire process and no additional shape modulators.

TEM images of sample HKUST-1-S is provided in the Supplementary Information in Fig. S1.

In Fig. 7 the dynamic light scattering plot is presented. For HKUST-1-N and HKUST-1-S samples, the particles size distribution can be distinguished into 2 maxima in the region of 15 μm and second one at around 330 and 480 μm. HKUST-1-S was characterized by rather lower particles than HKUST-1-N and the most dominant particle size of about 10 μm was consistent with SEM images (see Fig. 6). The particle size distribution of HKUST-1-Ac sample was more complex. For HKUST-1-Ac, 4 maxima can be seen at about 7, 50, 375, and 900 μm implying ununiform morphology of obtained material [55].

Surface concentrations of chemical bonds obtained from fitting XPS data for all analyzed samples are listed in Table S1 and in Fig. 8. The C 1s spectra were fitted with four lines: first one at 285.0 eV coming from aliphatic carbon C-C/C-H type bonds, second centered at 286.1 eV originating from organic C—O type bonds, third line centered at 288.9 eV coming from organic type C=O bonds and last line positioned at 290.9 eV which comes from O-C=O type bonds, originating from the organic linker [56–58] (Fig. 8a₁–c₁).

The O 1s spectra for all samples were fitted with two components:

first line centered at 532.0 eV which mainly comes from metal oxide (O—Cu) and O=C type bonds and second line found at 533.5 eV indicating O—C type bonds from organic material [59] (Fig. 8a₂–c₂).

The spectra collected at Cu 2p_{3/2} region are similar for HKUST-1-N and HKUST-1-S samples. HKUST-1-O on the other hand, exhibited nearly 60 % lower share of Cu⁰/Cu⁺ form and about 19 % higher share of Cu²⁺ form in comparison with HKUST-1-N. This phenomenon implies the impact of copper(II) salt precursor on the chemical bonds distribution during the HKUST-1 syntheses. Chemical state X-ray photoelectron spectroscopic analysis of copper species is challenging because of the complexity of the 2p spectra resulting from shake-up structures for Cu (II) species and overlapping binding energies for Cu metal and Cu(I) species. Here, each spectrum is fitted with six components with first line centered at 932.7 eV which points out the existence of Cu⁰/Cu⁺ oxidation state like in metallic copper or Cu₂O and due to the presence of shake-up structures found within binding energy range of 940–945 eV and additional left “shoulder” on spectra evidenced with the line centered at ~935 eV the Cu²⁺ oxidation state can be identified [60] (Fig. 8a₃–c₃).

3.2. Adsorption of chromium(III) ions

3.2.1. Adsorption kinetics

Adsorption kinetics allows to find the time needed to obtain saturation of adsorbent by removal of pollutant over its surface. The results are summarized in Table 4 and in Fig. 9. The potential application of obtained MOFs was evaluated by using them as adsorbents of Cr(III) ions

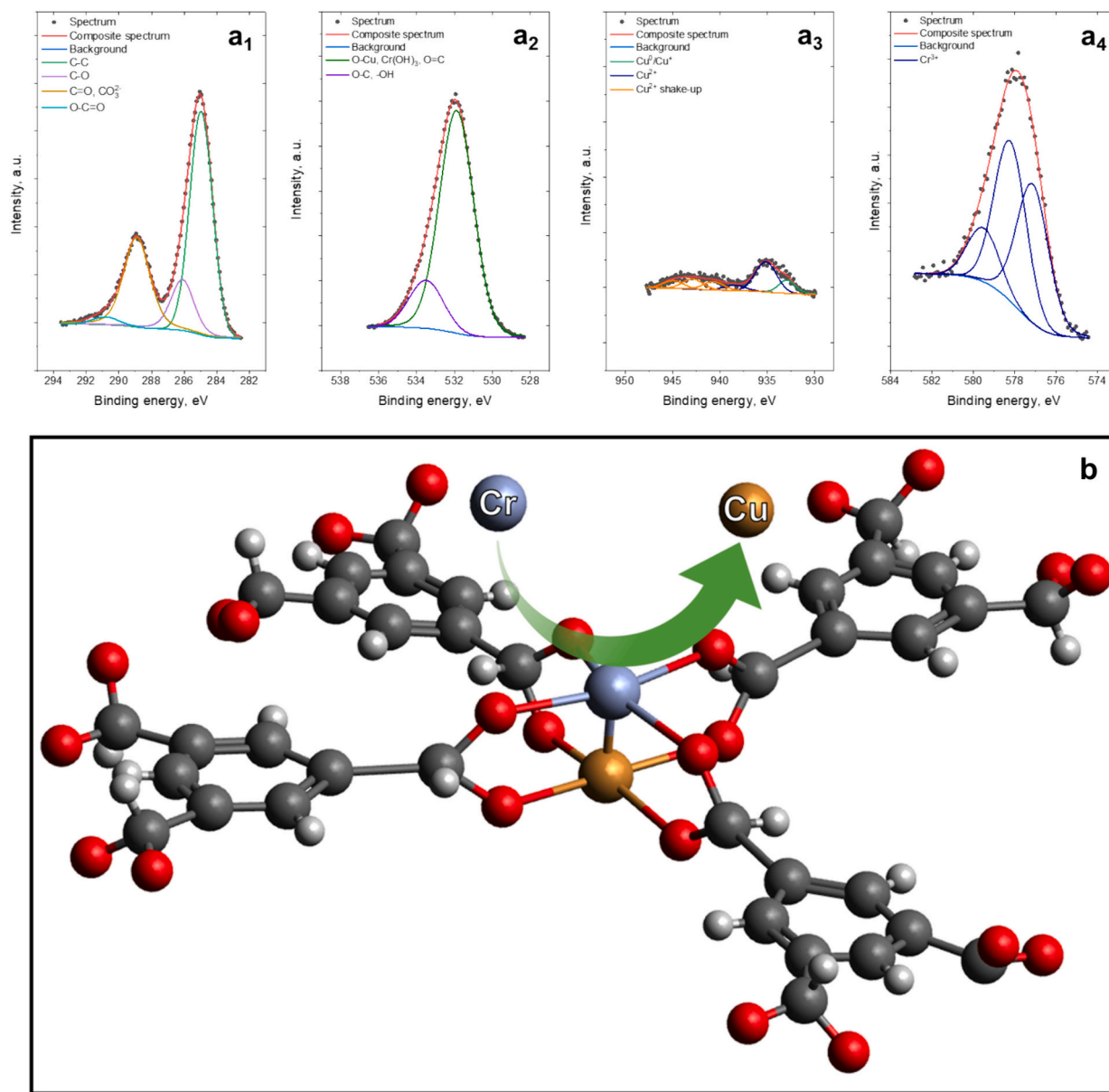


Fig. 11. XPS spectra of C 1s (a_1 - c_1), O 1s (a_2 - c_2), and Cu 2p (a_3 - c_3), and Cr 2p (a_4 - c_4) for HKUST-1-S (a) sample after adsorption, and visualization of the adsorption mechanism (b).

from aqueous solutions at pH of 5.00. For this pH value the potential competition between hydronium ions and Cr(III) ions is lower, than for pH in range from about 1 to 4, due to lower surface protonation [61]. On the other hand, for pH above 6, Cr(III) ions can precipitate from the solution [62]. Adsorption kinetics of Cr(III) ions was evaluated by comparison of experimental data with pseudo-first order, pseudo-second order, Elovich and Bangham models. It can be seen, that the pseudo-second order model fitted the best to the experimental data for all investigated samples in the series. The adsorption equilibrium was attained rather fast after just 120 min of adsorption. Familiar observation was evidenced for other materials like algae or aluminosilicate [63]. The highest adsorption capacity was obtained for HKUST-1-S and HKUST-1-N of 68.027 and 67.114 mg Cr(III) g^{-1} , respectively. Such high values might be related to the specific surface area of these materials (1790 and 1453 $m^2 g^{-1}$, respectively) and availability of adsorption centers over their surface. For HKUST-1-Ac the adsorption capacity was the lowest and reached 48.077 mg Cr(III) g^{-1} . Rather low correlation with Bangham model (<0.99) implies, that adsorption in pores was not

the limiting factor guiding the adsorption [64]. As for Elovich model, the correlation of the experimental data with was slightly >0.90 , which suggests that the adsorption was rather not multilayer [65].

3.2.2. Adsorption statics

Adsorption statics allows to investigate the effect of various pollution concentrations on the adsorption capacity of adsorbents. The results are summarized in Table 5 and in Fig. 10. The strongest correlation of experimental data was obtained for Langmuir model (>0.95 for all samples), rather than for Freundlich model (<0.88), implying that a monolayer adsorption occurred for investigated samples [35]. The maximum adsorption capacity (q_{max}) obtained for MOFs changed in order HKUST-1-S $>$ HKUST-1-N $>$ HKUST-1-Ac and equaled to 84.034, 79.923, and 46.512 mg g^{-1} , respectively. It appears, that the specific surface area had the most important factor on the obtained adsorption capacities for the materials.

The obtained results were compared with those in the literature. The comparison is presented in Table 6. The performance of investigated

MOFs is consistent with already reported materials.

3.2.3. Adsorption mechanism

Considering the potential mechanism of adsorption of Cr(III) ions by HKUST-1, it was evidenced by Zhao et al. [66], that high-valence cations like Cr(III) have higher bonding strength with the HKUST-1 active sites than lower-valence ions. On the other hand, in work of Zhao et al. [70], HKUST-1 was used as adsorbent of trivalent ions—cerium(III) from aqueous solution, implying a potential adsorption mechanism *via* ion exchange between Cu within the MOF structure and Ce(III) ions from the solution, instead of electrostatic attraction. In fact, chromium atom has smaller atom size (0.130 nm) than cerium atom (0.181 nm), which may effectively improve the ion exchange in the investigated adsorption process.

To understand the mechanism of Cr(III) ions adsorption using HKUST-1 MOFs, XPS analysis was conducted. The results are summarized in Fig. 11a₁-a₄ and Table S1. To confirm the hypothesis of the potential ion exchange occurring during the adsorption of Cr(III) ions, additional XPS analysis was performed using HKUST-1-S sample collected after the adsorption ($C_0 = 400 \text{ mg Cr(III) L}^{-1}$, pH = 5.00, dose 1 g L^{-1}). It can be clearly seen, that Cu species were significantly removed from the material (both Cu^0/Cu^+ and Cu^{2+} forms) and exchanged with Cr(III) ions. Total atomic % content of Cu was reduced by 87 % in comparison to parent HKUST-1-S sample (Table S1). An increase in the oxygen bindings share might suggest, that Cr(III) ions can be adsorbed also as hydroxide. The suspected mechanism of adsorption is presented in Fig. 11b. The spectra collected at Cr $2p_{3/2}$ region were fitted with three components with first line centered at 577.1 eV which indicate the existence of Cr^{3+} oxidation state. The two lines within energy range of 578–580 eV are due to the multiplet splitting phenomena [71].

4. Conclusions

MOFs type HKUST-1 were successfully synthesized using different copper(II) salt precursors. It was confirmed that the used precursor affected the physicochemical properties of the obtained MOFs in terms of their specific surface area, and surface morphology. Moreover, a synthesis free from DMF allows to obtain HKUST-1 MOF structure with desired properties. The solution pH (affected by the selected salt precursor) had rather negligible impact on the yield of MOFs, implying the importance of co-existing ions in the solution. Synthesis using copper(II) acetate allowed fast nucleation in comparison to other salt precursors, whereas copper(II) chloride yield no product after synthesis, which stays in line with the literature reports. The potential utility of obtained MOFs was confirmed in Cr(III) ions adsorption from aqueous solutions with adsorption capacity of 84.034 mg g^{-1} obtained for HKUST-1-S. Specific surface area of MOFs had the strongest effect on the obtained results, which suggests that adsorption active sites and ion exchange between Cu and Cr ions occur during the process. The adsorption mechanism was further confirmed *via* XPS analysis, which clearly indicated incorporation of Cr into the HKUST-1 structure. Greater specific surface area allowed better contact between Cr(III) ions from the solution and Cu(II) ions build into the HKUST-1 structure.

CRedit authorship contribution statement

Jakub Mokrzycki: Writing – review & editing, Writing – original draft, Visualization, Validation, Supervision, Software, Resources, Project administration, Methodology, Investigation, Funding acquisition, Formal analysis, Data curation, Conceptualization. **Eliza Wolak:** Writing – review & editing, Writing – original draft, Validation, Investigation, Formal analysis, Data curation. **Agnieszka Orzechowska-Zieba:** Writing – review & editing, Writing – original draft, Validation, Investigation, Formal analysis, Data curation. **Kun Zheng:** Validation, Software, Methodology, Investigation, Formal analysis, Data curation.

Dorota Duraczyńska: Visualization, Validation, Software, Methodology, Investigation, Formal analysis, Data curation. **Mateusz Marzec:** Data curation, Formal analysis, Investigation, Methodology, Software, Validation, Visualization. **Monika Fedyna:** Writing – review & editing, Visualization, Validation, Software, Methodology, Investigation, Formal analysis, Data curation.

Declaration of competing interest

The authors declare that they have no known competing financial interests or personal relationships that could have appeared to influence the work reported in this paper.

Data availability

Data will be made available on request.

Acknowledgement

This study was funded for subvention of AGH University of Krakow, Faculty Energy and Fuels (project No. 16.16.210.476).

Appendix A. Supplementary data

Supplementary data to this article can be found online at <https://doi.org/10.1016/j.jwpe.2024.105761>.

References

- [1] T. Saeed, A. Naeem, I. Ud Din, M.A. Alotaibi, A.I. Alharthi, I. Wali Khan, N. Huma Khan, T. Malik, Structure, nomenclature and viable synthesis of micro/nanoscale metal organic frameworks and their remarkable applications in adsorption of organic pollutants, *Microchem. J.* 159 (2020) 105579, <https://doi.org/10.1016/J.MICROC.2020.105579>.
- [2] J.Y.S. Lin, Molecular sieves for gas separation, *Science* 353 (2016) (1979) 121–122, <https://doi.org/10.1126/SCIENCE.AAG2267>.
- [3] C. Du, Z. Zhang, G. Yu, H. Wu, H. Chen, L. Zhou, Y. Zhang, Y. Su, S. Tan, L. Yang, J. Song, S. Wang, A review of metal organic framework (MOFs)-based materials for antibiotics removal via adsorption and photocatalysis, *Chemosphere* 272 (2021) 129501, <https://doi.org/10.1016/J.CHEMOSPHERE.2020.129501>.
- [4] K. Song, S. Liang, X. Zhong, M. Wang, X. Mo, X. Lei, Z. Lin, Tailoring the crystal forms of the Ni-MOF catalysts for enhanced photocatalytic CO₂-to-CO performance, *Appl Catal B* 309 (2022) 121232, <https://doi.org/10.1016/J.APCATB.2022.121232>.
- [5] Y. Shen, A. Tissot, C. Serre, Recent progress on MOF-based optical sensors for VOC sensing, *Chem. Sci.* 13 (2022) 13978–14007, <https://doi.org/10.1039/D2SC04314A>.
- [6] M. Ding, W. Liu, R. Gref, Nanoscale MOFs: from synthesis to drug delivery and theranostics applications, *Adv. Drug Deliv. Rev.* 190 (2022) 114496, <https://doi.org/10.1016/J.ADDR.2022.114496>.
- [7] X. Ma, L. Wang, H. Wang, J. Deng, Y. Song, Q. Li, X. Li, A.M. Dietrich, Insights into metal-organic frameworks HKUST-1 adsorption performance for natural organic matter removal from aqueous solution, *J. Hazard. Mater.* 424 (2022) 126918, <https://doi.org/10.1016/J.JHAZMAT.2021.126918>.
- [8] C. Chen, B. Li, L. Zhou, Z. Xia, N. Feng, J. Ding, L. Wang, H. Wan, G. Guan, Synthesis of hierarchically structured hybrid materials by controlled self-assembly of metal-organic framework with mesoporous silica for CO₂ adsorption, *ACS Appl. Mater. Interfaces* 9 (2017) 23060–23071, https://doi.org/10.1021/ACSAMI.7B08117/ASSET/IMAGES/LARGE/AM-2017-08117F_0016.JPEG.
- [9] J. Huo, M. Brightwell, S. El Hankari, A. Garai, D. Bradshaw, A versatile, industrially relevant, aqueous room temperature synthesis of HKUST-1 with high space-time yield, *J Mater Chem A Mater* 1 (2013) 15220–15223, <https://doi.org/10.1039/C3TA14409G>.
- [10] J. Sun, H.T. Kwon, H.K. Jeong, Continuous synthesis of high quality metal-organic framework HKUST-1 crystals and composites via aerosol-assisted synthesis, *Polyhedron* 153 (2018) 226–233, <https://doi.org/10.1016/J.POLY.2018.07.022>.
- [11] W.W. Lestari, R.E. Nugraha, I.D. Winarni, M. Adreane, F. Rahmawati, Optimization on electrochemical synthesis of HKUST-1 as candidate catalytic material for green diesel production, *AIP Conf. Proc.* 1725 (2016), <https://doi.org/10.1063/1.4945492/849849>.
- [12] V.I. Isaeva, V.I. Isaeva, B.R. Saifutdinov, V. V. Chernyshev, V. V. Chernyshev, V. V. Vergun, G.I. Kapustin, G.I. Kapustin, Y.P. Kurnysheva, M.M. Ilyin, L.M. Kustov, Impact of the Preparation Procedure on the Performance of the Microporous HKUST-1 Metal-Organic Framework in the Liquid-Phase Separation of Aromatic Compounds, *Molecules* 2020, Vol. 25, Page 2648 25 (2020) 2648. doi:<https://doi.org/10.3390/MOLECULES25112648>.

- [13] S. Qiu, J. Du, Y. Xiao, Q. Zhao, G. He, Hierarchical porous HKUST-1 fabricated by microwave-assisted synthesis with CTAB for enhanced adsorptive removal of benzothiophene from fuel, *Sep. Purif. Technol.* 271 (2021) 118868, <https://doi.org/10.1016/j.seppur.2021.118868>.
- [14] W. Zhang, M. Kauer, P. Guo, S. Kunze, S. Cwik, M. Muhler, Y. Wang, K. Epp, G. Kieslich, R.A. Fischer, Impact of synthesis parameters on the formation of defects in HKUST-1, *Eur. J. Inorg. Chem.* 2017 (2017) 925–931, <https://doi.org/10.1002/EJIC.201601239>.
- [15] J. Luczak, M. Kroczevska, M. Baluk, J. Sowik, P. Mazierski, A. Zaleska-Medynska, Morphology control through the synthesis of metal-organic frameworks, *Adv. Colloid Interface Sci.* 314 (2023) 102864, <https://doi.org/10.1016/j.cis.2023.102864>.
- [16] Y. Liu, B. Liu, Q. Zhou, T. Zhang, W. Wu, Morphology effect of metal-organic framework HKUST-1 as a catalyst on benzene oxidation, *Chem. Res. Chin. Univ.* 33 (2017) 971–978, <https://doi.org/10.1007/S40242-017-6468-4/METRICS>.
- [17] G. Majano, J. Pérez-Ramírez, G. Majano, J. Pérez-Ramírez, Scalable room-temperature conversion of copper(II) hydroxide into HKUST-1 (Cu₃(btc)₂), *Adv. Mater.* 25 (2013) 1052–1057, <https://doi.org/10.1002/ADMA.201203664>.
- [18] J.E. Lee, D.Y. Kim, H.K. Lee, H.J. Park, A. Ma, S.Y. Choi, D.S. Lee, Sonochemical synthesis of HKUST-1-based CuO decorated with Pt nanoparticles for formaldehyde gas-sensor applications, *Sens Actuators B Chem* 292 (2019) 289–296, <https://doi.org/10.1016/j.snb.2019.04.062>.
- [19] Y.K. Seo, G. Hundal, I.T. Jang, Y.K. Hwang, C.H. Jun, J.S. Chang, Microwave synthesis of hybrid inorganic-organic materials including porous Cu₃(BTC)₂ from cu(II)-trimesate mixture, *Microporous and Mesoporous Materials* 119 (2009) 331–337, <https://doi.org/10.1016/j.micromeso.2008.10.035>.
- [20] G.S. Deyko, L.M. Glukhov, V.I. Isaeva, V.V. Chernyshev, V.V. Vergun, D. A. Archipov, G.I. Kapustin, O.P. Tkachenko, V.D. Nissenbaum, L.M. Kustov, Modifying HKUST-1 crystals for selective ethane adsorption using ionic liquids as synthesis media, *Crystals (Basel)* 12 (2022) 279, <https://doi.org/10.3390/CRYST12020279/S1>.
- [21] M. Jin, X. Qian, J. Gao, J. Chen, D.K. Hensley, H.C. Ho, R.J. Percoco, C.M. Ritzl, Y. Yue, Solvent-free synthesis of CuO/HKUST-1 composite and its photocatalytic application, *Inorg. Chem.* 58 (2019) 8332–8338, https://doi.org/10.1021/ACS.INORGCHEM.9B00362/ASSET/IMAGES/LARGE/IC-2019-00362V_0007.JPEG.
- [22] V. Gargiulo, A. Pollicchio, L. Lisi, M. Alfe, CO₂ capture and gas storage capacities enhancement of HKUST-1 by hybridization with functionalized graphene-like materials, *Energy Fuels* 37 (2023) 5291–5302, https://doi.org/10.1021/ACS.ENERGYFUELS.2C04289/ASSET/IMAGES/LARGE/EF2C04289_0006.JPEG.
- [23] Y. Wen, W.H. Cheng, Y.R. Wang, F.C. Shen, Y.Q. Lan, Tailoring the Hydrophobic Interface of Core–Shell HKUST-1@Cu₂O Nanocomposites for Efficiently Selective CO₂ Electroreduction, *Small* 20 (2024) 2307467. doi:<https://doi.org/10.1002/SMLL.202307467>.
- [24] T. Laysandra, F. Edi Soetaredjo, J. Nyoo Putro, J. Lie, C. Gunarto, V. Bervia Lunardi, S. Permatasari Santoso, W. Irawaty, M. Yuliana, C. Julius Wijaya, I. Gede Wenten, S. Ismadji, Study of pharmaceutical contaminant adsorption using HKUST-1 as metal-organic framework model, *Environ Nanotechnol Monit Manag* 20 (2023) 100868, <https://doi.org/10.1016/j.enmm.2023.100868>.
- [25] H. Oliveira, F. Scacchetti, F. Bezerra, J. Santos, G. Soares, Comprehensive evaluation of HKUST-1 as an efficient adsorbent for textile dyes, *Environ. Sci. Pollut. Res.* 30 (2023) 87242–87259, <https://doi.org/10.1007/S11356-023-28455-3/FIGURES/10>.
- [26] P. Goyal, A. Paruthi, D. Menon, R. Behara, A. Jaiswal, K. V. A. Kumar, V. Krishnan, S.K. Misra, Fe doped bimetallic HKUST-1 MOF with enhanced water stability for trapping Pb(II) with high adsorption capacity, *Chem. Eng. J.* 430 (2022) 133088. doi:<https://doi.org/10.1016/j.cej.2021.133088>.
- [27] L. Xing, K.M. Haddao, N. Emami, F. Nalchifard, W. Hussain, H. jasem, A.H. Dawood, D. Toghraie, M. Hekmatifar, Fabrication of HKUST-1/ZnO/SA nanocomposite for doxycycline and naproxen adsorption from contaminated water, *Sustain. Chem. Pharm.* 29 (2022) 100757. doi:<https://doi.org/10.1016/j.scp.2022.100757>.
- [28] A. Ayele, Y.G. Godeto, Bioremediation of chromium by microorganisms and its mechanisms related to functional groups, *J. Chem.* 2021 (2021), <https://doi.org/10.1155/2021/7694157>.
- [29] Chromium in drinking-water Background document for development of. <http://apps.who.int/bookorders>, 2020. (Accessed 8 May 2024).
- [30] E. Vaiopoulou, P. Gikas, Regulations for chromium emissions to the aquatic environment in Europe and elsewhere, *Chemosphere* 254 (2020) 126876, <https://doi.org/10.1016/j.chemosphere.2020.126876>.
- [31] O.M. Ontañón, P.S. González, G.G. Barros, E. Agostini, Improvement of simultaneous Cr(VI) and phenol removal by an immobilized bacterial consortium and characterisation of biodegradation products, *N. Biotechnol.* 37 (2017) 172–179, <https://doi.org/10.1016/j.nbt.2017.02.003>.
- [32] S. Kirmızı, B. Karabacakoglu, Performance of electrodialysis for Ni(II) and Cr(VI) removal from effluents: effect of process parameters on removal efficiency, energy consumption and current efficiency, *J. Appl. Electrochem.* 53 (2023) 2039–2055, <https://doi.org/10.1007/S10800-023-01894-Z/TABLES/3>.
- [33] N. Bin Darwish, A. AlAlawi, Hexavalent chromium removal from aqueous solution by polymer-enhanced ultrafiltration, *Chem. Eng. Commun.* 211 (2024) 736–742, <https://doi.org/10.1080/00986445.2023.2291801>.
- [34] J. El Gaayda, Y. Rachid, F.E. Titchoh, I. Barra, A. Hsini, P.S. Yap, W. Da Oh, C. Swanson, M. Hamdani, R.A. Akbour, Optimizing removal of chromium (VI) ions from water by coagulation process using central composite design: effectiveness of grape seed as a green coagulant, *Sep. Purif. Technol.* 307 (2023) 122805, <https://doi.org/10.1016/j.seppur.2022.122805>.
- [35] J. Mokrzycki, I. Michalak, P. Rutkowski, Tomato green waste biochars as sustainable trivalent chromium sorbents, *Environ. Sci. Pollut. Res.* 28 (2021) 24245–24255, <https://doi.org/10.1007/S11356-019-07373-3/FIGURES/6>.
- [36] E.M.C. Morales, M.A. Méndez-Rojas, L.M. Torres-Martínez, L.F. Garay-Rodríguez, I. López, I.E. Uflyand, B.I. Kharisov, Ultrafast synthesis of HKUST-1 nanoparticles by solvothermal method: properties and possible applications, *Polyhedron* 210 (2021) 115517, <https://doi.org/10.1016/j.poly.2021.115517>.
- [37] V. Stavila, J. Volponi, A.M. Katzenmeyer, M.C. Dixon, M.D. Allendorf, Kinetics and mechanism of metal-organic framework thin film growth: systematic investigation of HKUST-1 deposition on QCM electrodes, *Chem. Sci.* 3 (2012) 1531–1540, <https://doi.org/10.1039/C2SC20065A>.
- [38] S. Amirjalayer, M. Tafipolsky, R. Schmid, Surface termination of the metal-organic framework HKUST-1: a theoretical investigation, *J. Phys. Chem. Lett.* 5 (2014) 3206–3210, https://doi.org/10.1021/JZ5012065/SUPPL_FILE/JZ5012065_SI_004.PDF.
- [39] F. Li, M. Ao, G.H. Pham, J. Sunarso, Y. Chen, J. Liu, K. Wang, S. Liu, Cu/ZnO Catalysts Derived from Bimetallic Metal-Organic Framework for Dimethyl Ether Synthesis from Syngas with Enhanced Selectivity and Stability, *Small* 16 (2020) 1906276. doi:<https://doi.org/10.1002/SMLL.201906276>.
- [40] I. Youssef, S. Sall, T. Dintzer, S. Labidi, C. Petit, I. Youssef, S. Sall, T. Dintzer, S. Labidi, C. Petit, Forward looking analysis approach to assess copper acetate thermal decomposition reaction mechanism, *Am J Analyt Chem* 10 (2019) 153–170, <https://doi.org/10.4236/AJAC.2019.105014>.
- [41] D. Jiang, C. Huang, J. Zhu, P. Wang, Z. Liu, D. Fang, Classification and role of modulators on crystal engineering of metal organic frameworks (MOFs), *Coord. Chem. Rev.* 444 (2021) 214064, <https://doi.org/10.1016/j.ccr.2021.214064>.
- [42] H. Guo, Y. Zhu, S. Wang, S. Su, L. Zhou, H. Zhang, Combining coordination modulation with acid-base adjustment for the control over size of metal-organic frameworks, *Chem. Mater.* 24 (2012) 444–450, https://doi.org/10.1021/CM202593H/ASSET/IMAGES/LARGE/CM202593H_SI_001.PDF.
- [43] S.E. Crawford, K.J. Kim, Y. Yu, P.R. Ohodnicki, Rapid, selective, ambient growth and optimization of copper Benzene-1,3,5-Tricarboxylate (cu-BTC) metal-organic framework thin films on a conductive metal oxide, *Cryst. Growth Des.* 18 (2018) 2924–2931, https://doi.org/10.1021/ACS.CGD.8B00016/ASSET/IMAGES/LARGE/CG-2018-00016P_0004.JPEG.
- [44] S. Loera-Serna, H.I. Beltrán, M. Mendoza-Sánchez, J.C. Álvarez-Zeferino, F. Almanza, F. Fernández-Luqueño, Effect of HKUST-1 metal-organic framework in root and shoot systems, as well as seed germination, *Environ. Sci. Pollut. Res.* 31 (2024) 13270–13283, <https://doi.org/10.1007/S11356-023-31728-6/TABLES/4>.
- [45] M. Thommes, K. Kaneko, A.V. Neimark, J.P. Olivier, F. Rodriguez-Reinoso, J. Rouquerol, K.S.W. Sing, Physisorption of gases, with special reference to the evaluation of surface area and pore size distribution (IUPAC technical report), *Pure Appl. Chem.* 87 (2015) 1051–1069, <https://doi.org/10.1515/PAC-2014-1117/MACHINEREADEABLECITATION/RIS>.
- [46] P. Chowdhury, C. Bikkina, D. Meister, F. Dreisbach, S. Gumma, Comparison of adsorption isotherms on cu-BTC metal organic frameworks synthesized from different routes, *Microporous Mesoporous Mater.* 117 (2009) 406–413, <https://doi.org/10.1016/j.micromeso.2008.07.029>.
- [47] Y. Chen, X. Mu, E. Lester, T. Wu, High efficiency synthesis of HKUST-1 under mild conditions with high BET surface area and CO₂ uptake capacity, *Prog. Nat. Sci.: Mater. Int.* 28 (2018) 584–589, <https://doi.org/10.1016/j.pnsc.2018.08.002>.
- [48] P. Goyal, A. Paruthi, D. Menon, R. Behara, A. Jaiswal, K. V. A. Kumar, V. Krishnan, S.K. Misra, Fe doped bimetallic HKUST-1 MOF with enhanced water stability for trapping Pb(II) with high adsorption capacity, *Chem. Eng. J.* 430 (2022) 133088. doi:<https://doi.org/10.1016/j.cej.2021.133088>.
- [49] A.S. Khder, M. Morad, H.M. Altass, A.A. Ibrahim, S.A. Ahmed, Unprecedented green chemistry approach: tungstophosphoric acid encapsulated in MOF 199 as competent acid catalyst for some significant organic transformations, *J. Porous. Mater.* 28 (2021) 129–142, <https://doi.org/10.1007/S10934-020-00973-2/TABLES/4>.
- [50] N. Farzaneh, F. Radinekiyan, M.R. Naimi-Jamal, M.G. Dekamin, Development of new magnetic nanocomposite designed by reduced graphene oxide aerogel and HKUST-1, and its catalytic application in the synthesis of polyhydroquinoline and 1,8-dioxo-decahydroacridine derivatives, *Scientific Reports* 2023 13:1 13 (2023) 1–15. doi:<https://doi.org/10.1038/s41598-023-48674-5>.
- [51] P.C. Lemaire, J. Zhao, P.S. Williams, H.J. Walls, S.D. Shepherd, M.D. Losego, G. W. Peterson, G.N. Parsons, Copper Benzenetricarboxylate metal-organic framework nucleation mechanisms on metal oxide powders and thin films formed by atomic layer deposition, *ACS Appl. Mater. Interfaces* 8 (2016) 9514–9522, https://doi.org/10.1021/ACSAMI.6B01195/ASSET/IMAGES/LARGE/AM-2016-01195F_0010.JPEG.
- [52] D. Garg, H. Rekhi, H. Kaur, K. Singh, A.K. Malik, A novel method for the synthesis of MOF-199 for sensing and photocatalytic applications, *J. Fluoresc.* 32 (2022) 1171–1188, <https://doi.org/10.1007/S10895-022-02902-9/TABLES/3>.
- [53] A. Domán, J. Madarász, K. László, In situ evolved gas analysis assisted thermogravimetric (TG-FTIR and TG/DTA-MS) studies on non-activated copper benzene-1,3,5-tricarboxylate, *Thermochim. Acta* 647 (2017) 62–69, <https://doi.org/10.1016/j.tca.2016.11.013>.
- [54] P.S. Ho, K.C. Chong, S.O. Lai, S.S. Lee, W.J. Lau, S.Y. Lu, B.S. Ooi, Synthesis of cu-BTC metal-organic framework for CO₂ capture via solvent-free method: effect of metal precursor and molar ratio, *Aerosol Air Qual. Res.* 22 (2022) 220235, <https://doi.org/10.4209/AAQR.220235>.
- [55] J. Shen, W. Zhou, M. Jia, X. Yang, J. Lin, L. An, Q. Tian, S. Yang, Tumor microenvironment-responsive reagent DFS@HKUST-1 for photoacoustic imaging-guided multimethod therapy, *ACS Appl. Bio Mater.* 4 (2021) 5753–5764, <https://doi.org/10.1021/acsapb.1c00000>.

- doi.org/10.1021/ACSABM.1C00521/ASSET/IMAGES/LARGE/MT1C00521_0005.JPEG.
- [56] D. (David) Briggs, Surface analysis of polymers by XPS and static SIMS, (1998) 198. https://books.google.com/books/about/Surface_Analysis_of_Polymers_by_XPS_and.html?hl=pl&id=HnXhXoxE1OgC (accessed June 19, 2024).
- [57] J.R. Rumble, D.M. Bickham, C.J. Powell, The NIST x-ray photoelectron spectroscopy database, *Surf. Interface Anal.* 19 (1992) 241–246, <https://doi.org/10.1002/SIA.740190147>.
- [58] X. Cui, X. Sun, L. Liu, Q. Huang, H. Yang, C. Chen, S. Nie, Z. Zhao, Z. Zhao, In-situ fabrication of cellulose foam HKUST-1 and surface modification with polysaccharides for enhanced selective adsorption of toluene and acidic dipeptides, *Chem. Eng. J.* 369 (2019) 898–907, <https://doi.org/10.1016/j.cej.2019.03.129>.
- [59] NIST X-ray Photoelectron Spectroscopy Database, (n.d.). <https://srdata.nist.gov/xps/EnergyTypeElement> (accessed June 19, 2024).
- [60] M.C. Biesinger, Advanced analysis of copper X-ray photoelectron spectra, *Surf. Interface Anal.* 49 (2017) 1325–1334, <https://doi.org/10.1002/SIA.6239>.
- [61] Y. Zhang, X. Xu, C. Yue, L. Song, Y. Lv, F. Liu, A. Li, Insight into the efficient co-removal of Cr(VI) and Cr(III) by positively charged UiO-66-NH₂ decorated ultrafiltration membrane, *Chem. Eng. J.* 404 (2021) 126546, <https://doi.org/10.1016/j.cej.2020.126546>.
- [62] J. Liu, X. Wu, Y. Hu, C. Dai, Q. Peng, D. Liang, Effects of Cu(II) on the adsorption behaviors of Cr(III) and Cr(VI) onto kaolin, *J. Chem.* 2016 (2016), <https://doi.org/10.1155/2016/3069754>.
- [63] I. Michalak, S. Baśladyńska, M. Mularczyk, K. Marycz, Investigation on the potential sorbents — Aluminosilicate, microalga and grass hay as feed additives, *Environ. Technol. Innov.* 24 (2021) 101816, <https://doi.org/10.1016/j.ETI.2021.101816>.
- [64] J. Mokrzycki, E. Lorenc-Grabowska, K. Kordek-Khalil, P. Rutkowski, Hydrothermal and pyrolytic biochars from waste milk thistle (*Silybum marianum*) extrudates as precursors for production of effective isoproturon adsorbents, *Journal of Water Process Engineering* 37 (2020) 101459, <https://doi.org/10.1016/j.jwpe.2020.101459>.
- [65] W. Wang, K. Rouibah, H. Ferkous, M. Abdessalam-Hassan, B.L. Mossab, A. Boublia, C. Pierlot, A. Abdennouri, I. Avramova, M. Alam, Y. Benguerba, A. Erto, Exploring the Efficiency of Algerian Kaolinite Clay in the Adsorption of Cr(III) from Aqueous Solutions: Experimental and Computational Insights, *Molecules* 2024, Vol. 29, Page 2135–29 (2024) 2135. doi:<https://doi.org/10.3390/molecules29092135>.
- [66] L. Zhao, X. Duan, M.R. Azhar, H. Sun, X. Fang, S. Wang, Selective adsorption of rare earth ions from aqueous solution on metal-organic framework HKUST-1, *Chemical Engineering Journal Advances* 1 (2020) 100009, <https://doi.org/10.1016/j.cej.2020.100009>.
- [67] Y. Zheng, Y. Li, L. Huang, H. Nan, Y. Wu, A facile fabrication of MOF for selective removal of chromium (III) from aqueous solution, *J. Dispers. Sci. Technol.* 40 (2019) 918–924, <https://doi.org/10.1080/01932691.2018.1489278>.
- [68] B. Dash, S.K. Jena, S.S. Rath, Adsorption of Cr (III) and Cr (VI) ions on muscovite mica: experimental and molecular modeling studies, *J. Mol. Liq.* 357 (2022) 119116, <https://doi.org/10.1016/j.molliq.2022.119116>.
- [69] J. Mokrzycki, I. Michalak, P. Rutkowski, Biochars obtained from freshwater biomass—green macroalga and hornwort as Cr(III) ions sorbents, *Biomass Convers. Biorefinery* 11 (2021) 301–313, <https://doi.org/10.1007/S13399-020-00649-6/TABLES/7>.
- [70] L. Zhao, M.R. Azhar, X. Li, X. Duan, H. Sun, S. Wang, X. Fang, Adsorption of cerium (III) by HKUST-1 metal-organic framework from aqueous solution, *J. Colloid Interface Sci.* 542 (2019) 421–428, <https://doi.org/10.1016/j.jcis.2019.01.117>.
- [71] B.P. Payne, M.C. Biesinger, N.S. McIntyre, X-ray photoelectron spectroscopy studies of reactions on chromium metal and chromium oxide surfaces, *J Electron Spectrosc Relat Phenomena* 184 (2011) 29–37, <https://doi.org/10.1016/j.elspec.2010.12.001>.